Monatshefte für Chemie - Chemical Monthly
https://doi.org/10.1007/s00706-018-2302-z

ORIGINAL PAPER

A facile synthesis of formazan dyes conjugated with plasmonic nanoparticles as photosensitizers in photodynamic therapy against leukemia cell line

Mohamed E. Khalifa[1] · Elham A. Elkhawass[2] · Antoni Pardede[3,4] · Masayuki Ninomiya[3] · Kaori Tanaka[5,6] · Mamoru Koketsu[3]

Received: 9 May 2018 / Accepted: 25 September 2018

Abstract

A series of 1,5-bis(4-aryl/heteryl)-3-cyanoformazan derivatives was synthesized and characterized by spectral analysis. The synthesis strategy involved an easy and practical diazo coupling of different aryl (heteryl) diazonium salts with cyanoacetic acid. The synthesized compounds were electrostatically conjugated to gold and/or silver nanoparticles in dimethylsulfoxide and were examined as photosensitizers for photodynamic therapy (PDT). The PDT activity of the formazan derivatives alone and conjugated with metal nanoparticles was investigated against HL-60 cells under dark and light conditions. Formazan derivatives and their conjugates showed variable promising anticancer activity in dark and light conditions related to their structures. The interaction of synthesized formazan derivatives with metal nanoparticles enhanced the light absorption of the dyes and thus showed remarkable increase in PDT against cancer cells.

Graphical abstract

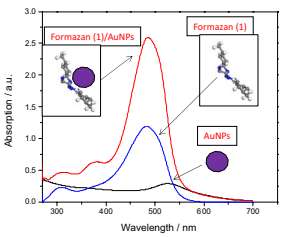

Keywords Diazo compounds · Photochemistry · Antitumor agents · Formazans · Leukemia · Photodynamic therapy

✉ Mohamed E. Khalifa
mohamedezzat200@hotmail.com

[1] Department of Chemistry, University of Taif, Taif 21974, Saudi Arabia

[2] Department of Zoology, Faculty of Science, Suez Canal University, Ismailia 41522, Egypt

[3] Department of Chemistry and Biomolecular Science, Faculty of Engineering, Gifu University, 1-1 Yanagido, Gifu 501-1193, Japan

[4] Department of Chemistry Education, Islamic University of Kalimantan, JI, Adhyaksa No. 2 Kayu Tangi, Banjarmasin 70123, Indonesia

[5] Division of Anaerobe Research, Life Science Research Center, Gifu University, 1-1 Yanagido, Gifu 501-1194, Japan

[6] United Graduate School of Drug Discovery and Medicinal Information Sciences, Gifu University, 1-1 Yanagido, Gifu 501-1194, Japan

Published online: 26 October 2018

Introduction

Formazans are an important and distinct class of organic compounds with the general formula R–N=N–C(R′)=NNHR″. The chemistry of formazans has attracted the interest due to their wide biological activities such as antimicrobial, antiviral, anti-oxidant, analgesic, anti-inflammatory, anticonvulsant, antiparkinsonian, antiproliferative, anthelmintic, antitubercular, and cardiovascular, while some formazans have been tested for their anticancer and anti-HIV activities and found to be inactive [1]. Formazans have a wide range of industrial applications as well as their utility in analytical chemistry and synthesis of heterocyclic compounds [1–3]. Generally, three reported synthetic strategies are often used for preparation of formazans. The first strategy involves coupling of aldehyde hydrazones with diazonium salts to synthesize symmetrical and asymmetrical formazans. The second strategy involves coupling of active methylene or methine compounds with two molar equivalents of diazonium salts for the synthesis of only symmetrical *N,N′*-disubstituted formazans. The third strategy involves oxidation of the hydrazidines with the proper hydrazine derivatives [4–7]. The second strategy is easiest and highly practical; however, the substituents at the carbon atom are limited to non-aromatic structures, where the basicity of the medium, ratio of reagent, and type of substituent play key roles in this reaction [8].

Photodynamic therapy (PDT) and photothermal therapy (PTT) are important tools for cancer therapy as well as many other diseases [9]. The mechanism of PDT action is based upon the production of reactive oxygen species (ROS) through the interaction between light and photosensitizer dye (PSD) molecules [10, 11]. The transfer of energy from the photo-excited PSD molecules to oxygen generates ROS. Cytotoxicity of ROS species causes oxidative cell death. PTT in contrary to PDT does not need oxygen species, because the light-activated sensitizer releases energy as vibration thermal energy (heat). The generated heat is able to kill the cancer cells. There is a new trend of combining PDT with PTT to overcome the limitation of PDT, where the synergistic effect of PTT with PDT, has potentials to increase the efficiency of PDT treatments. Conjugations of different nanoparticles like gold nanoparticles and graphene oxide with PSD molecules are used to enhance anticancer effect using synergistic PDT/PTT [12–14]. The photosensitization of toluidine blue for example, was enhanced by conjugation with gold nanomaterials, where the effect was probably due to increase of the extinction coefficient of the dye in the UV–visible absorption region by the gold nanoparticles [15]. Silver nanoparticles are one of the most interesting metal nanoparticles that were recently involved in anticancer research [16]. In many studies, silver nanoparticles were investigated for their cytotoxicity against cancer cells. Antitumor effects of silver nanoparticles (AgNPs) were reported against lung cancer H1299 cells, breast cancer cells, prostatic cancer PPC-1 cells, and larynx cancer cell (Hep-2 cell lines) [17–19]. Many studies showed that cancer cells were more susceptible to AgNPs than normal ones, and cancer cell death is related to apoptotic effect of AgNPs which is arbitrated by a ROS mechanism via mitochondria [20, 21]. In addition, the anticancer activity of AgNPs against cancer cell is increased by increasing the dose and decreasing the particle size [17, 22]. In the current investigation, we report the interaction of some formazan dye derivatives with metal nanoparticles (gold and/or silver) synthesized in DMSO as a solvent. A great advantage of our approach is to use a formazan–metal nanoparticles conjugate system where each component will provide a sufficient backup for the partner limitations compared to the individual use of metal nanoparticles or formazans in PDT.

Results and discussion

Formazan dyes' synthesis

In this work, the targeted photosensitizer agents 1,5-bis(4-aryl/heteryl)-3-cyanoformazans **1**–**7** were synthesized via reaction of two equivalents of the appropriate aryl (heteryl) diazonium salt with deprotonated cyanoacetic acid, where the reaction proceeded upon attack of the diazonium cation by the in situ-generated carbanion of cyanoacetic acid. The hydrazone-type intermediates were then deprotonated (by hydroxide) and the resulting carbanion attacked a second equivalent of aryl diazonium cation resulting in accepted yields of compounds **1**–**7** (Scheme 1). The carboxyl group associated with cyanoacetic acid must be lost during the

Scheme 1

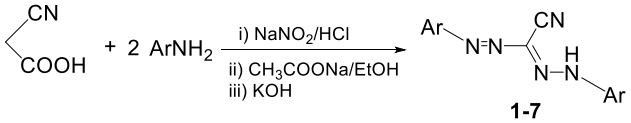

	Ar
1	C_6H_4-CH_3(*p*)
2	C_6H_4-OCH_3(*p*)
3	C_6H_4-OH(*p*)
4	C_6H_4-$COCH_3$(*p*)
5	C_6H_4-COOH(*p*)
6	C_6H_4-NO_2(*p*)
7	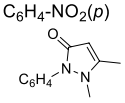

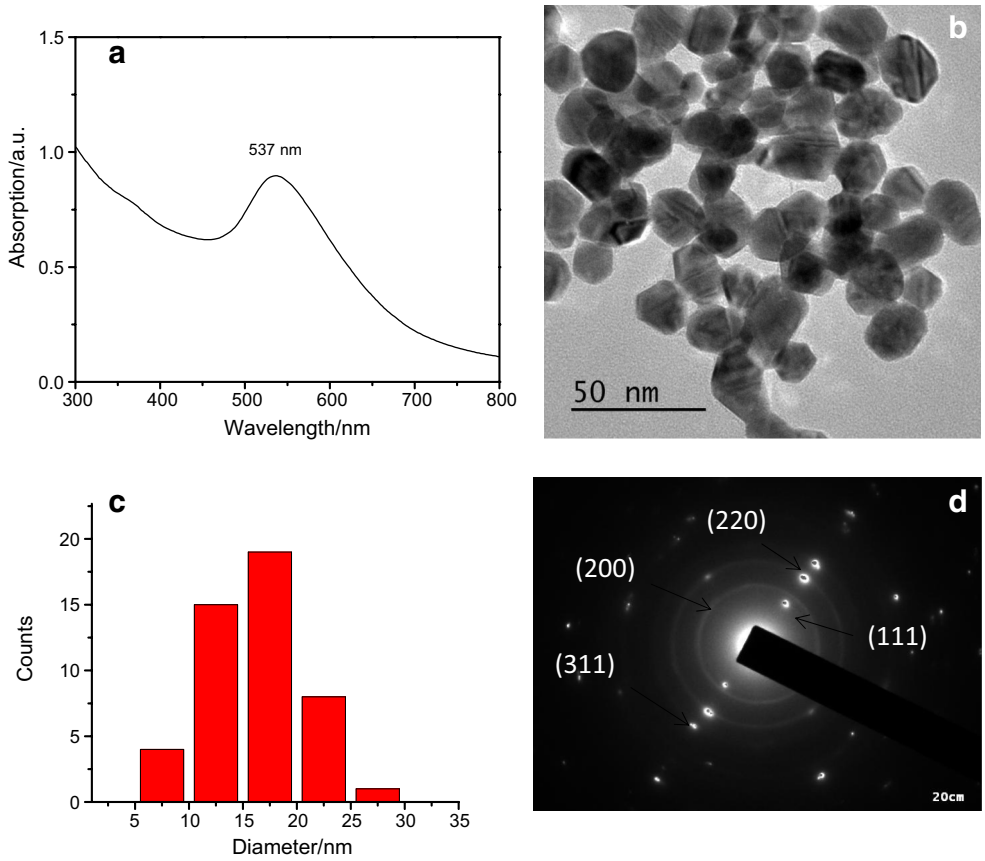

Fig. 1 **a** UV–Vis absorbance of AuNPs prepared in DMSO; **b** HRTEM images of AuNPs; **c** particle size distribution of AuNPs; **d** selected area electron diffraction (SAED)

reaction (probably as CO_2), although it is not clear at which stage this occurs [23].

Dyes' characterizations

The IR spectra of all synthesized formazans **1**–**7** were recorded, where the azo groups (–N=N–) appeared at the range 1488–1600 cm^{-1} and cyano group (C≡N) at the range 2184–2232 cm^{-1}. The observation of N–H bands at the range 3172 and 3404 cm^{-1} indicated the absence of the intramolecular hydrogen bonding in formazans. Proton NMR spectra have been used extensively to elucidate the structure of synthesized formazans. The chemical shifts of the aromatic protons were recorded between 6.69 and 8.45 ppm as expected. Methoxy protons ($–OCH_3$) were observed as a singlet at 3.85 ppm, whereas methyl groups ($–CH_3$) were detected in the upfield (2.40–2.58 ppm). IR, ^1H NMR, ^{13}C NMR, and mass spectra confirmed the validity of the structures given in Scheme 1 and in good agreement with the reported literature values [24–28].

Metal nanoparticles' characterization

The presence of gold nanoparticles in DMSO was confirmed by UV–Vis spectra. Figure 1a showed the UV–Vis spectra of gold nanoparticles (AuNPs) in DMSO. The surface plasmon band appeared at 537 nm, confirming the presence of AuNPs. The high-resolution transmission electron microscope (HRTEM) images (Fig. 1b) showed lattice fringes representing atomic layers with measured lattice *d*-spacing of 0.236 nm consistent with (111) diffraction plans. The size of AuNPs was estimated to be with average diameter 17 ± 11 nm as shown in Fig. 1c. The selected area electron diffraction (SAED) pattern (Fig. 1d) showed the concentric spots representing 111, 200, 220, and 311 reflection planes of face-centered cubic (fcc) gold structure.

The presence of silver nanoparticles in DMSO was confirmed by UV–Vis spectra. Figure 2a shows UV–Vis absorption spectrum of AgNPs in DMSO. The surface plasmon band appeared at 425 nm, confirming the production of AgNPs. The high-magnified HRTEM images showed silver nanoparticles with average diameter 9 nm (Fig. 2c). The high-magnified HRTEM images (Fig. 2b) showed lattice

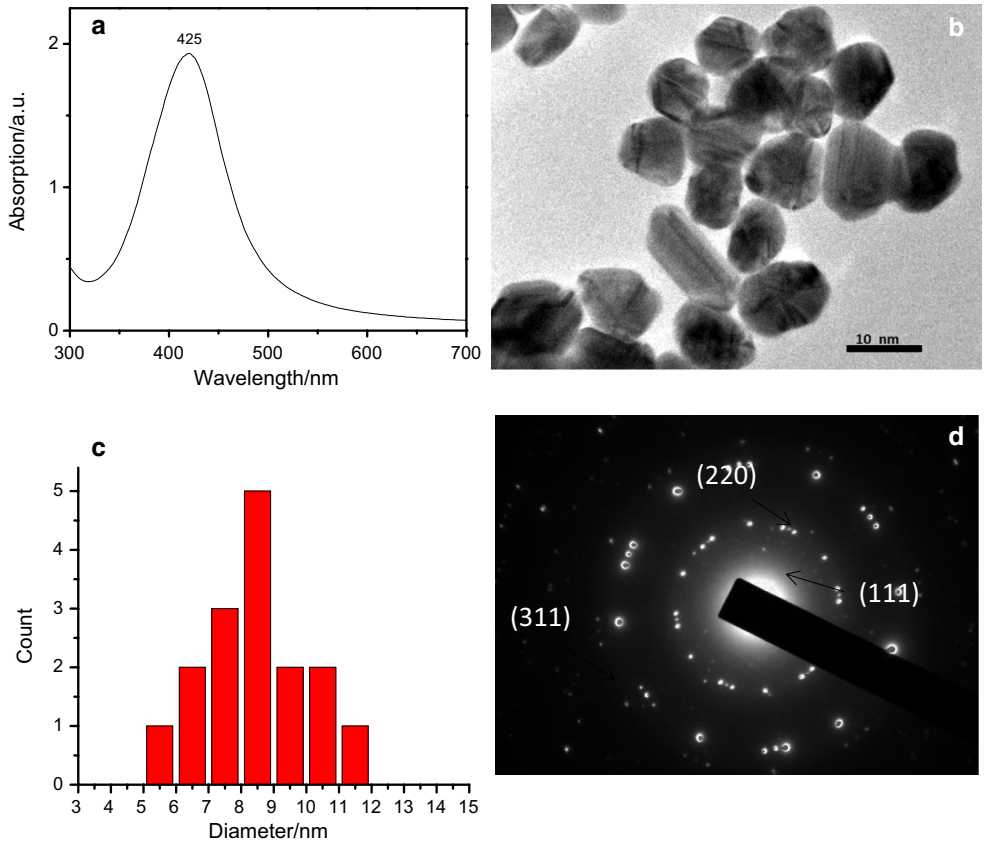

Fig. 2 **a** UV–Vis absorbance of AgNPs prepared in DMSO; **b** HRTEM images of AgNPs; **c** particle size distribution of AgNPs; **d** selected area electron diffraction (SAED)

fringes representing atomic layers with measured lattice *d*-spacing of 0.22 nm consistent with (111) diffraction plans. The SAED pattern (Fig. 2d) showed the concentric spots representing 111, 200, and 311 reflection planes of face-centered cubic (fcc) silver structure.

Interaction of dyes with metal nanoparticles

The surface of gold and silver nanoparticles interacted electrostatically with photosensitizer dyes and was ascertained by UV–Vis spectroscopy (Figs. 3, 4). The absorbance spectra of formazan dye derivatives (shown in blue) and their conjugate with AuNPs or AgNPs (shown in red) in compression with AuNPs and/or AgNPs alone (shown in black). For better illustrating the effect of metal nanoparticles on absorption spectra of the dyes, we added curves representing subtraction of the absorbance spectrum of the metal nanoparticles from that of the dye/nanoparticle conjugates (shown in green). The UV–Vis spectra of formazans were investigated experimentally and theoretically [29, 30]. The reported maximum absorption values were determined at 400–550 nm and it can be shifted to 570–650 nm depending on the presence of side-electron-withdrawing groups [29, 31]. In the present investigation, the UV–Vis absorption spectrum of formazan dyes in DMSO solvent showed two bands, one strong and one weak (Figs. 3, 4). The strong band is due to the energetically favorable $\pi \rightarrow \pi^*$ electron transition, which occurs due to electron transfer from the highest energy bonding π-orbital (HOMO) to the lowest energy antibonding π-orbital (LUMO). The weak band is due to $n \rightarrow \pi^*$ electron transition [30].

Table 1 summarizes the determined electronic absorption maxima; λ_{max1} and λ_{max2}, before conjugation and after conjugation with metal nanoparticles, respectively. Formazans **1**, **2**, **6**, and **7** showed λ_{max1} at higher wave lengths than λ_{max2}. However, formazans **3**, **4**, and **5** showed the reverse, where λ_{max1} at lower wave lengths than λ_{max2}. Thus, it is expected that formazans **1**, **2**, **6**, and **7** to show better PDT than other dyes, because their absorption maxima are close to the therapeutic window (600–800 nm) and the start of the absorption bands extend to the therapeutic window.

Although, there were no remarkable shifts in absorption maxima; λ_{max1} and λ_{max2}, some dyes showed remarkable increase in the absorption bands' intensities after interaction with metal surfaces. This observation was obvious for **1**, **2**, and **6** in both AuNPs and AgNPs conjugations (Figs. 3, 4).

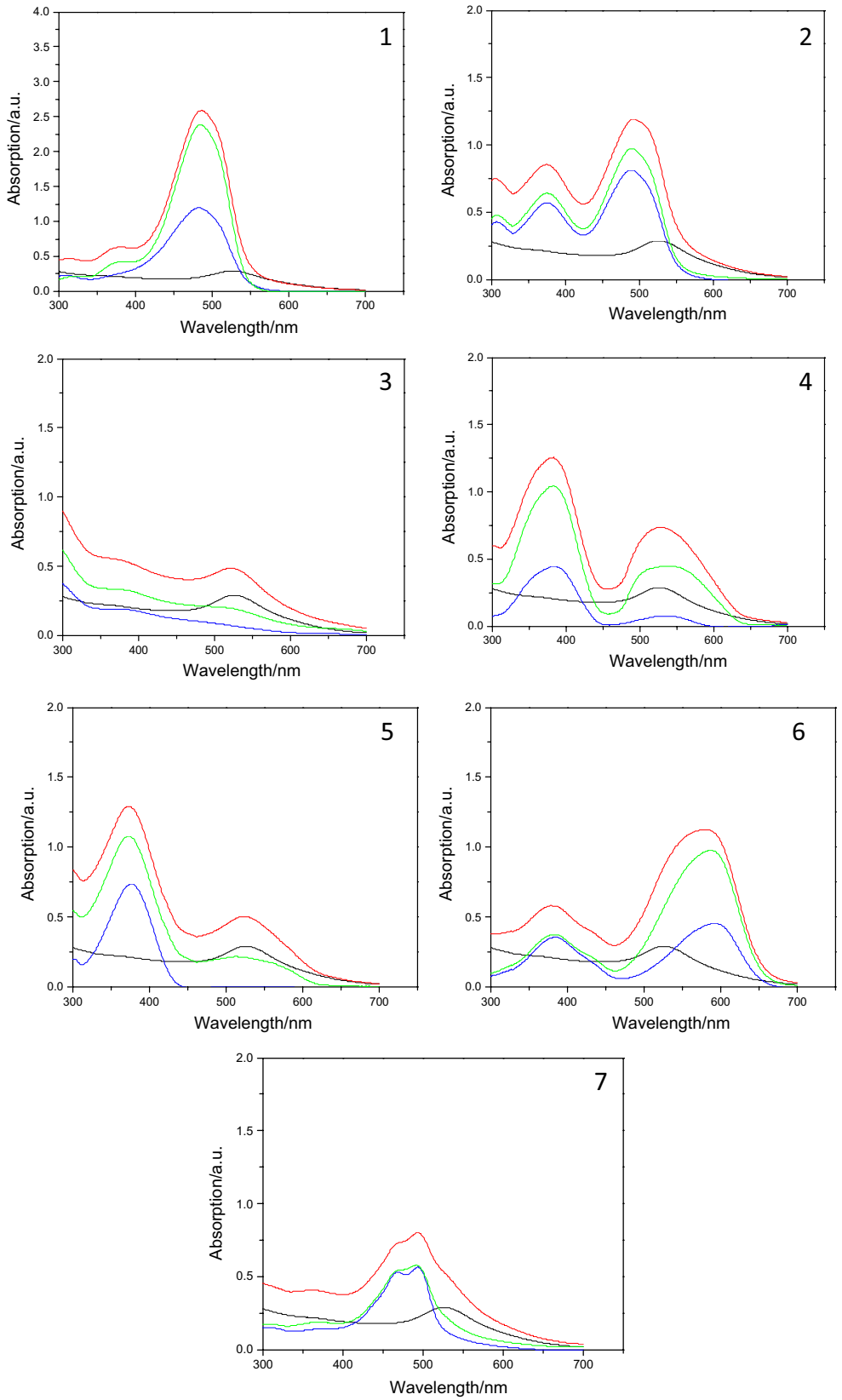

Fig. 3 UV–Vis absorption spectra of AuNPs (black curves), dyes (blue curves), dyes–AuNPs (red curves) and the difference between dyes/AuNPs and AuNPs (green curves); AuNPs concentration = 0.1 mM (as Au) and dyes concentration = 0.0125 mM (color figure online)

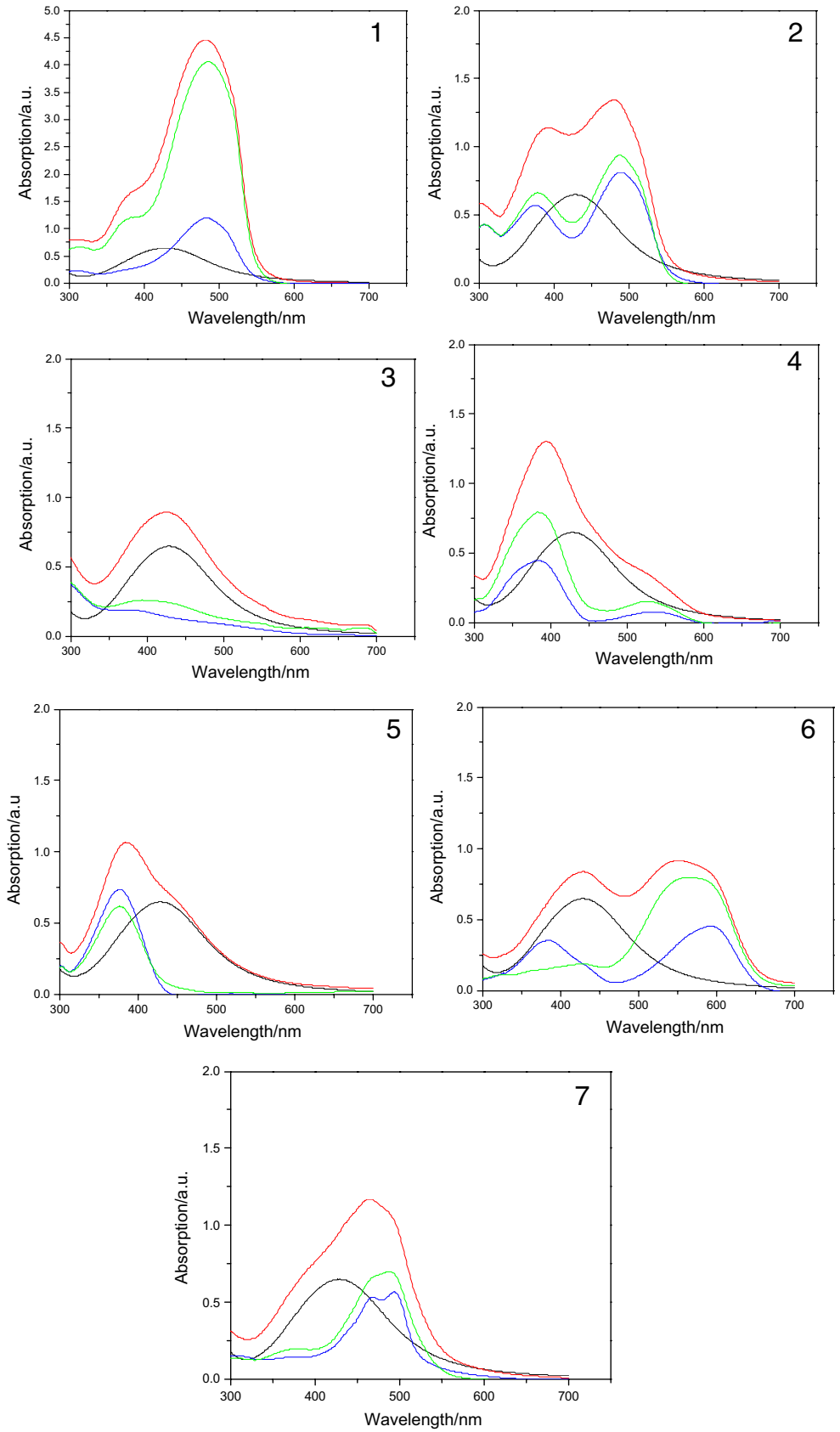

Fig. 4 UV–Vis absorption spectra of AgNPs (black curves), dyes (blue curves), dyes–AgNPs (red curves) and the difference between dyes/AgNPs and AgNPs (green curves); AgNPs concentration = 0.1 mM (as Ag) and dyes concentration = 0.0125 mM (color figure online)

Table 1 Experimentally determined electronic absorption maxima; λ_{max} before conjugation and after conjugation with metal nanoparticles

	Dye		Dye/AuNPs		Dye/AgNPs	
	λ_{max1}/nm	λ_{max2}/nm	λ_{max1}/nm	λ_{max2}/nm	λ_{max1}/nm	λ_{max2}/nm
1	484	376	484	376	497	384
2	488	375	492	375	488	375
3	291	377	291	378	291	378
4	381	530	281	532	381	530
5	300	378	300	378	300	383
6	593	385	593	385	593	385
7	495	469	495	469	495	469

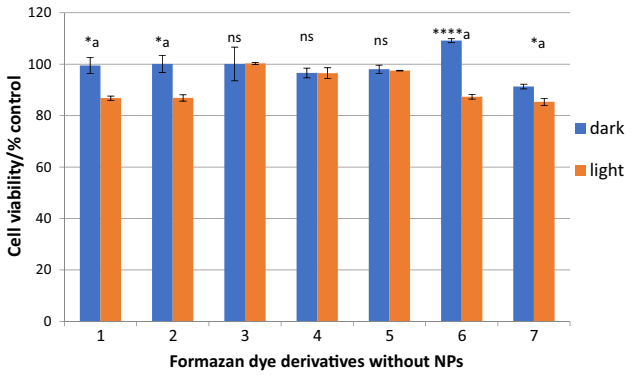

Fig. 5 In vitro cytotoxicity of formazan dye derivatives without metal nanoparticles on human promyelocytic leukemia cells (HL-60) under dark and light conditions. Statistical differences; ns, no significant differences, $*P < 0.05$, $**P < 0.01$, $***P < 0.001$, $****P < 0.0001$ using paired *t* test. **a** Significant at light condition

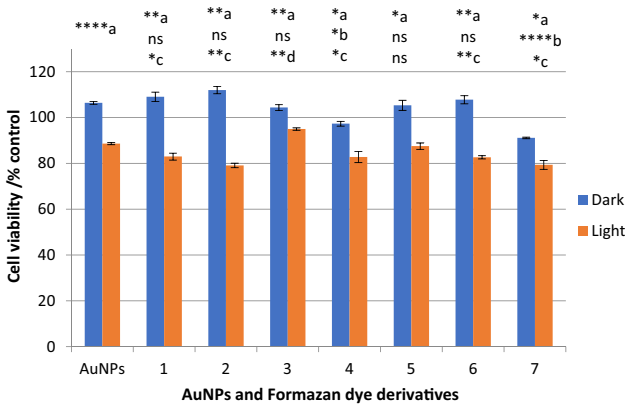

Fig. 6 In vitro cytotoxicity of AuNPs alone and formazan dye derivatives conjugated with AuNPs on human promyelocytic leukemia cells (HL-60) under dark and light conditions. Statistical differences; ns, no significant differences, $*P < 0.05$, $**P < 0.01$ and $****P < 0.0001$ using paired *t* test. **a** Comparing each variable alone at both light conditions; **b** comparing formazan dyes/AuNPs conjugates with AuNPs alone at dark condition; **c** significant for formazan dyes/AuNPs conjugates compared to AuNPs alone at light condition; **d** significant for AuNPs alone compared to formazan dyes/AuNPs conjugates at light condition

Enhanced optical absorption of dye molecules in the vicinity of metallic nanomaterials was proved [32]. The insignificant shifts in absorption maxima; λ_{max1} and λ_{max2}, are due to weak van der Waal adsorption interactions between dyes and metals surfaces [33]. The maximum observed increase in absorption band intensity was for dye **1** after conjugation with AgNPs (**1**/AgNPs conjugate), as shown in Fig. 4.

Photodynamic activity against human promyelocytic leukemia cells (HL-60)

Cytotoxicity and photodynamic activity of formazan dye derivatives on human promyelocytic leukemia cells (HL-60) were estimated in the presence and absence of AuNPs and AgNPs under light/dark condition. Cytotoxicity of formazan derivatives without nanoparticles at dark and light conditions was shown in Fig. 5. At dark condition, only formazan derivative **7** shows obvious cytotoxicity as compared to other derivatives. However, at light conditions, dyes derivatives **1**, **2**, **6**, and **7** showed high phototoxicity ($P < 0.05$ for **1**, **2**, and **7** and $P < 0.0001$ for **6**). While other formazan dye derivatives showed insignificant differences in both their dark and light cytotoxicity against HL-60 cells (Fig. 5).

Figure 6 shows the dark/light cytotoxicity of formazan/AuNPs conjugates and AuNPs alone. Initially, cytotoxicity of AuNPs alone under light is very highly significant than under dark condition ($P < 0.0001$). The effect of light condition on the cell viability of these derivatives in presence of AuNPs revealed high phototoxicity of all formazan derivatives. Moreover, a remarkable dark cytotoxicity was observed for **7**/AuNPs conjugates. Comparing phototoxicity of previously mentioned derivatives versus that of AuNPs alone show highly significant phototoxicity at **1**, **2**, **4**, **6**, **7**/AuNPs conjugates. However, phototoxicity of AuNPs alone is highly significant as compared to **3**/AuNPs conjugate ($P < 0.01$). On the other hand, under dark condition, comparing cytotoxicity of earlier derivatives versus that of AuNPs alone shows no significant differences in their cytotoxicity at **1**, **2**, **3**, **5**, and **6**. There is only higher dark cytotoxicity of **4** and **7**/AuNPs conjugates compared to AuNPs alone ($P <$ 0.05 and 0.0001, respectively).

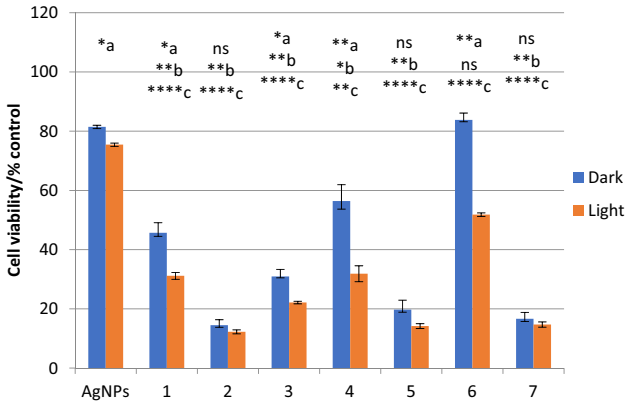

Fig. 7 In vitro cytotoxicity of AgNPs alone and formazan dye derivatives conjugated with AgNPs on human promyelocytic leukemia cells (HL-60) under dark and light conditions. Statistical differences of formazan/AgNPs conjugates; ns, no significant difference, $*P < 0.05$, $**P < 0.01$, and $****P < 0.0001$ using paired *t* test. **a** Comparing each variable alone at both light conditions; **b** comparing formazan dyes/AgNPs conjugates with AgNPs alone at dark condition; **c** comparing formazan dyes/AgNPs conjugates with AgNPs alone at light condition

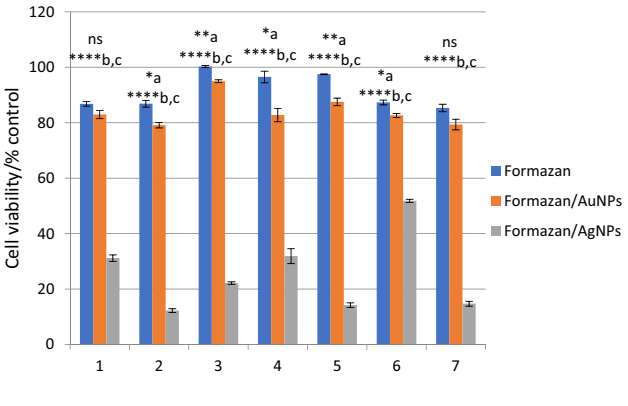

Fig. 8 In vitro phototoxicity of formazan dye derivatives alone, formazan dye derivatives/AuNPs conjugates, and formazan dye derivatives/AgNPs conjugates on human promyelocytic leukemia cells (HL-60). Statistical differences; $*P < 0.05$, $**P < 0.01$, $***P < 0.001$, $****P < 0.0001$, using paired *t* test; ns, no significant differences between formazan dye alone compared to formazan/AuNPs conjugates; **a** statistical differences in favor of formazan/AuNPs conjugates compared to formazan dye derivatives alone; **b** statistical differences in favor of formazan/AgNPs conjugates compared to formazan dye derivatives alone; **c** statistical differences in favor of formazan/AgNPs conjugates compared to formazan/AuNPs conjugates

Figure 7 showed the dark/light cytotoxicity of formazan/AgNPs conjugates and AgNPs alone. Comparing cytotoxicity of AgNPs alone on cancerous cells under both luminosity condition show significant difference in favor of light one ($P < 0.05$). Generally, all formazan/AgNPs conjugates show high cytotoxicity at both dark and light conditions. At dark condition, the cytotoxicity of formazan/AgNPs in descending order was **2**/AgNPs < **7**/AgNPs < **5**/AgNPs < **3**/AgNPs < **1**/AgNPs < **4**/AgNPs < **6**/AgNPs. In addition, all formazan/AgNPs conjugates except conjugate **6** show highly significant dark cytotoxicity as compared to AgNPs cytotoxicity alone. Similarly, all formazan/AgNPs conjugates reveal highly significant phototoxicity as compared to AgNPs phototoxicity alone. Additionally, Formazan derivatives **1**, **3**, **4**, and **6**/AgNPs conjugates showed high phototoxicity, in comparison with their dark cytotoxicity ($P < 0.05$, 0.05, 0.01, and 0.01, respectively).While **2**, **5**, and **7** conjugates with AgNPs showed no significant differences between both light and dark cytotoxicity.

Assessment of nanoparticles' effect on the cytotoxicity of formazan derivatives against cancerous cells was compared under the same luminosity condition, as shown in Figs. 8 and 9. Figure 8 showed the phototoxicity of formazan derivatives alone and conjugated with gold nanoparticles and/or silver nanoparticles. Formazan/AuNPs conjugates **2**, **3**, **4**, **5**, and **6** show high significant cytotoxicity compared to formazan derivatives alone ($P < 0.05$ for **2**, **4**, and **6**, and $P < 0.01$ for **3** and **5**). While formazan/AuNPs conjugates (**1** and **7**) showed insignificant cytotoxicity compared to formazan derivatives alone. Moreover, all formazan/AgNPs conjugates induced

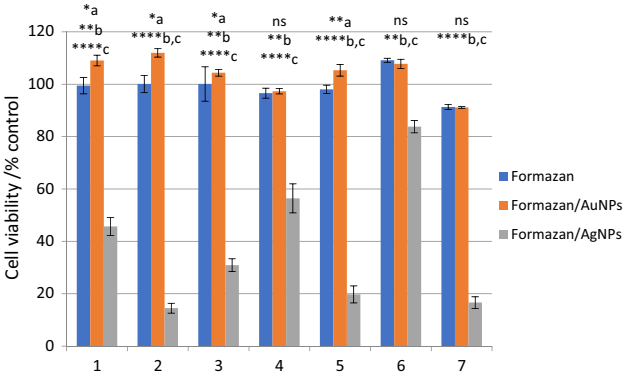

Fig. 9 In vitro dark-cytotoxicity of formazan dye derivatives alone, formazan dye derivatives/AuNPs conjugates, and formazan dye derivatives/AgNPs conjugates on human promyelocytic leukemia cells (HL-60). Statistical differences; $*P < 0.05$, $**P < 0.01$, $***P < 0.001$, $****P < 0.0001$, using paired *t* test; ns, no significant differences between formazan dye alone compared to formazan/AuNPs conjugates; **a** statistical differences in favor of formazan dye derivatives alone compared to formazan/AuNPs conjugates; **b** statistical differences in favor of formazan/AgNPs conjugates compared to formazan dye derivatives alone; **c** statistical differences in favor of formazan/AgNPs conjugates compared to formazan/AuNPs conjugates

very highly significant phototoxicity against leukemia cells compared to formazan derivatives alone ($P < 0.0001$ for all).

Figure 9 shows the dark cytotoxicity of formazan derivatives alone and conjugated with gold nanoparticles or silver nanoparticles. Under dark condition, formazan derivatives **1**,

2, **3**, and **5** show high cytototoxicity compared to formazan/AuNPs conjugates. While **4**, **6**, and **7** derivatives showed insignificant differences as compared to formazan/AuNPs conjugates. Interestingly, formazan/AgNPs conjugates showed also high dark-cytotoxicity compared to formazan derivatives alone ($P < 0.01$ for **1**, **3**, **4**, and **6** and $P < 0.0001$ for **2**, **5**, and **7**). Comparing cytotoxicity of formazan derivatives conjugated with gold and silver nanoparticles showed that the cytotoxicity of formazan/AgNPs conjugates was higher than formazan/AuNPs conjugates at both dark and light conditions.

Discussion

Conventional cancer therapy still cannot keep up with such elevated cancer rates besides the well-known side-effects of these treatments. Thus, researchers are working on developing more successful treatments such as PDT [34]. Since the 1990s, a broad variety of dye sensitizers have been engineered for PDT of several diseases and cancers [35, 36]. In accordance with this study, effect of luminosity on the cytotoxicity of formazan derivatives alone or conjugated with AuNPs or AgNPs against leukemia revealed the potential phototoxicity of these conjugated systems.

Low-density lipoprotein (LDL) considers the major carrier lipoprotein for cholesterol in human plasma via receptor-mediated endocytosis called LDL receptors [37]. Many investigations showed that high LDL-cholesterol levels are a key factor in cancer cells' progression and control [37, 38]. Leukemic cells from patients with acute myelogenous leukemia have highly elevated LDL receptors that enhance the uptake of lipophilic chemotherapy drugs to leukemic cells [39]. In this study, we suggest that water-insoluble formazan dye derivatives without metal nanoparticles are likely to be delivered as LDL–dye sensitizer complexes to tumor cells as explained by Ormond [36]. Previously mentioned LDL–dye complex mostly will likely to be accumulated internally in mitochondria as a cationic compound as described by Malik [40].

Formazan **7** was found to be the only derivative that showed obvious dark cytotoxicity to cancer cell, although all previous studies conducted on formazans did not show any significant anticancer effect [1, 2, 41–43]. This may due to the presence of antipyrine moiety at the skeleton of this derivative, which had been proved to have anticancer activity [44]. Formazan derivatives **1**, **2**, **6**, and **7** showed high phototoxicity ($P < 0.05$ for **1**, **2**, and **7** and $P < 0.0001$ for **6**) without metal nanoparticles. The high phototoxicity of these derivatives is due to the high wave lengths of their absorption maxima (λ_{max1}) in comparison with other derivatives. Moreover, their absorption bands start at much higher wave lengths (565, 686, 675, and 636 nm, respectively). As expected from UV–Vis spectra, these derivatives showed PDT effect because their intense absorption band started above 600 nm, which is in the rage of therapeutic window (600–900 nm). Formazan derivatives **1**, **2**, and **6** presented ideal rational photosensitizers for PDT, especially because of their dark cytotoxicity [36]. The other formazan dye derivatives showed no significant differences in their photo cytotoxicity against HL-60 cells. However, derivative **7** showed both dark and light cytotoxicity.

Drug delivery systems using nanoparticles grant higher drug uptake and passive accumulation by cancerous cells [45, 46]. In this probe, we suggest that using noble metal nanoparticles as AgNPs and AuNPs enhance dye/nanoparticles delivery and accumulation in tumor cells besides their cytotoxicity with/without photosensitization. Under normal cultural conditions without photosensitization, many investigations revealed that AgNPs works as an independent therapeutic agent with multiple mechanisms of cytotoxicity [47–50] and as a highly enhanced therapeutic agent with radiation [51]. In addition, Kovács et al. [52] established synergistic relation of AgNPs with different chemotherapy drugs on drug-resistant cancer cells. Similarly, formazan/AgNPs conjugates revealed high dark-cytotoxicity indicating the promising potential of AgNPs as anticancer agent and of formazan/AgNPs conjugates due to electrostatic interaction that likely promotes formazan/AgNPs delivery to cancer cells. Additionally, formazan/AgNPs conjugates are highly promising agents against leukemia as compared to formazan/AuNPs conjugates, both in dark and light conditions.

Moreover, formazan/AgNPs conjugates revealed high dark-cytotoxicity indicating the promising potential of AgNPs alone as anticancer agent that is confirmed also by the high cytotoxicity of formazan/AgNPs conjugates as compared to formazan/AuNPs conjugates both in dark and light conditions. Formazan/AgNPs conjugates showed high phototoxicity against leukemia as compared to formazan derivatives alone or to formazan/AuNPs conjugates. AgNPs were known to cause uncontrolled mitochondrial function and provoked apoptosis and/or necrosis that explained the high cytotoxicity of formazan/AgNPs conjugates [47, 48]. Wang et al. [53] showed that silver nanoparticles conjugated with hematoporphyrin IX molecule leads to high ROS production under photosensitization, although, the same conjugate shows low cytotoxicity without photosensitization. El-Hussein et al. [54] found that the photodynamic activity of AgNPs was higher than that of AuNPs. The unsystematic cytotoxicity of formazan/AgNPs conjugates is due to the different mechanisms of cell killing, where the formazan dyes and AgNPs have PDT as well as the dissolved silver ion may take part, which shows cytotoxicity against cancer cells in many investigations [16, 18, 19, 49, 55, 56]. Other studies show that cancer cells are more susceptible to AgNPs than normal cells and cell death is related to apoptotic effect of

AgNPs which is arbitrated by a ROS mechanism via mitochondria [20, 50]. The phototoxicity of these formazan conjugates is high under light condition suggesting the high photodynamic activity of these dyes-conjugate due to generation of ROS [57]. As explained by this study, the metal nanoparticles have enhanced the optical absorption of the synthesized dyes which in agreement with literature [58].

Conclusion

A synthesis of a series of mono azo compounds of 1,5-bis(4-aryl/heteryl)-3-cyanoformazan derivatives **1**–**7** using the more practical and easier strategy was performed. The synthesized compounds were charged to gold and silver nanoparticles in DMSO and have been applied as photosensitizers for use in photodynamic therapy (PDT) against leukemia cell lines. The phototoxic activities of some formazan derivatives were improved after conjugation with metal nanoparticles (AuNPS and AgNPs) due to the significant enhancement in the absorption intensities of the dyes and the shift in the start of their absorption bands inside the therapeutic window. The PDT efficiency of dye–metal nanoparticle conjugates depended on the structure of the formazan dye derivatives as well as the enhancement of UV absorption was assumed to be due to the conjugation. Generally, formazan electrostatic conjugates with AgNPs showed higher cytotoxicity than those with AuNPs in both dark and light conditions due to the combined action of the formazan derivatives and silver nanoparticles previously discussed.

Experimental

The reagents were of analytical grade or chemically pure. Elemental analyses (C, H, N) were conducted using the PerkinElmer 2400 Analyzer, series II (PerkinElmer Co., Shelton, UK); their results were found to be in good agreement (±0.3%) with the calculated values. All of the corrected melting points were determined using a Stuart SMP20 melting point apparatus (Bibby Scientific Limited, Staffordshire, UK). The infrared spectra were recorded on a PerkinElmer Alpha platinum-ATR spectrometer, and the ^{1}H NMR spectra were measured on a JOEL ECS-400 (JOEL Ltd., Tokyo, Japan) in $CDCl_3$ and DMSO-d_6 using TMS as an internal standard. The surface properties of metal nanoparticles were analyzed using a transmission electron microscope (1200 EX, JOEL Inc, Peabody, MA, USA). The microanalyses, spectral analyses and nanoparticles' analyses were performed at the Micro Analytical Centers of Taif University, Saudi Arabia (IR, CHN, Nanoparticles characterization) and Gifu University, Japan (^{1}H NMR, ^{13}C NMR, and mass spectra). The biological assessment was performed at Life Science Research Center, Gifu University, Japan.

General method for the synthesis of 1,5-bis(4-substituted phenyl)-3-cyanoformazan derivatives 1–7

Coupling of 1:2 molar ratio of cyanoacetic acid with different diazotised aromatic amines (*p*-toluidine, *p*-anisidine, *p*-aminophenol, *p*-aminoacetophenone, *p*-aminobenzoic acid, *p*-nitrophenol, and *p*-aminoantipyrine) in sodium acetate and ethanol at 0–5 °C was performed to obtain the corresponding derivatives of 1,5-bis(4-aryl)-3-cyanoformazan **1**–**7**. The reaction mixture was neutralized by adding 10% potassium hydroxide solution dropwise. The precipitate which formed was collected by filtration, dried, and recrystallized from proper solvent. The IR, ^{1}H NMR, ^{13}C NMR, and mass spectra for the obtained compounds were recorded to characterise the structure of these compounds. Compounds **1**, **2**, and **4**–**7** were characterized according to the literature procedures [24–28, 59].

1,5-Bis(4-methylphenyl)-3-cyanoformazan (1) Orange solid; yield 58%; m.p.: 212–214 °C (MeOH) (198–200 °C [24], 216–217 °C [25]).

1,5-Bis(4-methoxyphenyl)-3-cyanoformazan (2) Red solid; yield 56%; m.p.: 151–152 °C (EtOH) (150–152 °C [24]).

1,5-Bis(4-hydroxyphenyl)-3-cyanoformazan (3, $C_{14}H_{11}N_5O_2$) Reddish brown solid; yield 53%; m.p.: > 230 °C (dioxan); IR: = 1497 (C–N str.), 1577 (N=N), 2220 (CN), 3172 (NH str.), 3350 (OH, broad) cm^{-1}; ^{1}H NMR (400 MHz, DMSO-d_6): δ = 6.69–7.32 (m, 8H, aromatic), 6.76 (s, 1H, OH), 12.92 (s, 1H, NH) ppm; ^{13}C NMR (100 MHz, DMSO-d_6): δ = 149.4 (2C–benzene–OH), 146.3 (C=N imine), 137.5 (C–N), 130.2 (2C–benzene), 135.2 (C–NH), 119.5 (2C–benzene), 117.8 (2C–benzene), 116.6 (2C–benzene), 116.5 (C-nitrile) ppm; MS (EI): *m/z* = 282.00 (M^+, 68%); HRMS: *m/z* calc. for $C_{14}H_{11}N_5O_2$ 281.0913, found 281.0925.

1,5-Bis(4-acetylphenyl)-3-cyanoformazan (4) Yellowish brown solid; yield 70%; m.p.: 180–182 °C (EtOH) (228 °C (acetic acid) [26]).

1,5-Bis(4-carboxyphenyl)-3-cyanoformazan (5) Yellow solid; yield 53%; m.p.: 228–230 °C (dioxan/DMF) (> 450 °C [27]).

1,5-Bis(4-nitrophenyl)-3-cyanoformazan (6) Reddish brown solid; yield 71%; m.p.: 210–212 °C (dioxan) (218–219 °C [28]).

1,5-Bis(4-antipyrinyl)-3-cyanoformazan (7) Reddish brown solid; yield 57%; m.p.: 215–216 °C (EtOH) (143 °C [59]).

Synthesis and characterization of gold and silver nanoparticles

Three stock solutions of chloroauric acid (50 mM), silver nitrate (50 mM), and trisodium citrate (5%) were prepared as follows: solution A: 0.5900 g of $HAuCl_4 \cdot 3H_2O$ (1.500 mmol) was dissolved in 30 cm^3 DMSO; solution B: 0.2550 g of $AgNO_3$ (1.500 mmol) was dissolved in 30 cm^3 DMSO; and solution C: 0.5 g $Na_3C_6H_5O_7 \cdot 2H_2O$ was dissolved in 10 cm^3 deionized water.

Synthesis of gold nanoparticles

2.0 cm^3 of solution A (50 mM) was added to 48 cm^3 DMSO to give 2 mM solution and heated under reflux. The solution was boiled for 5 min with continuous stirring. 1 cm^3 of solution C was added, and the mixture was boiled for a further 15 min. The color changed from yellow to colorless then to wine-red. The reaction was allowed to cool to room temperature.

Synthesis of silver nanoparticles

2.0 cm^3 of solution B (50 mM) was added to 48 cm^3 of DMSO to give 2 mM solution and heated under reflux. The solution was boiled for 5 min with continuous stirring. 1 cm^3 of solution C was added, and the mixture was boiled for a further 15 min. The color changed from colorless to yellow. The reaction was allowed to cool to room temperature.

Conjugation of the dyes with metal nanoparticles

Conjugation of formazan dye derivatives to freshly prepared metal nanoparticles was carried out according to the following steps. The volume of all mixtures was kept constant and equal to 4.0 cm^3. The concentrations of AuNPs and AgNPs were kept at 0.1 mM (as Au or Ag) and the concentration of dye was kept at 0.0125 mM. The concentration ratio of the dye and metal nanoparticles was selected to have no/or minimum free dyes and was set constant for comparison. The metal nanoparticles or dye/metal nanoparticles solutions were characterized by spectroscopic and microscopic studies and used in the cytotoxicity experiments. To obtain UV–Vis spectra of in-house prepared gold and silver nanoparticles, they were scanned in range of 200–900 nm using a double beam spectrophotometer. TEM and nanophox particle analysis were used to study the morphological features and size of the particles. The surface properties of metal nanoparticles were analyzed using a transmission electron microscope (1200 EX, JOEL Inc, Peabody, MA, USA), where samples were prepared by putting a drop of the metal nanoparticles on a carbon-coated copper grid and then dried in air before being transferred to the transmission electron microscope.

Biological assessment

Cell culture

HL-60 cells (DS Pharma Biomedical Co., Ltd., Osaka, Japan) were cultured in RPMI 1640 media (Wako Pure Chemical Industries, Ltd., Osaka, Japan) supplemented with 10% heat-inactivated fetal bovine serum (FBS) and 1% antibiotics, penicillin–streptomycin (Gibco®, Life Technologies, Thermo Fisher Scientific Inc., MA, USA). Cells were maintained at 37 °C under a humidified atmosphere of 5% CO_2.

CCK-8 assay

Cell counting kit-8 (CCK-8) was purchased from Dojindo Molecular Technologies, Inc. (Kumamoto, Japan). HL-60 cells (5×10^4 cells/cm^3, 100 mm^3) were seeded in 96-well plates. After 24-h incubation, solutions of test samples (300 μM) were added into the culture. Following 2-h incubation under the halogen lamp and/or dark conditions, CCK-8 solution (10 mm^3) was added, and the plates were incubated for an additional 3 h. Visible absorption (490 nm) was measured using a microplate reader (E_{max} precision microplate reader, Molecular Devices Japan, Tokyo, Japan).

Irradiation conditions

The USHIO lighting JDR 50 lamp spectrum, (110 V, 40 WLW/K, beam angle 35°, USHIO lighting Co., Japan) was used for irradiation and temperature was kept at 37 °C. The wavelength of the lamp ranges from 350 to 800 nm with total light dose 77 J/cm^2 [60].

Statistical analysis

Microsoft Excel software was used for raw data conversion. All data were expressed as average ± SD. Differences between different experimental trails; treated only with formazan dye derivatives and treated with formazan dye derivatives conjugated with gold and/or silver nanoparticles in presence and absence of light were evaluated using paired *t* test by IBM SPSS Statistics.

References

1. Shawali AS, Samy NA (2015) J Adv Res 6:241
2. Barltrop JA, Owen TC, Cory AH, Cory JG (1991) Bioorg Med Chem Lett 1:611

3. Kidwai M, Negi N, Gupta SD (1994) Chem Pharm Bull 42:2363
4. Buzykin BI (2010) Chem Heterocycl Compd 46:379
5. Buzykin BI (2010) Chem Heterocycl Compd 46:1043
6. Abbas AA, Elwahy AHM (2009) Arkivoc 2009:65
7. Ibrahim YA, Abbas AA, Elwahy AHM (2004) J Heterocycl Chem 41:135
8. Katritzky AR, Belyakov SA, Cheng D, Durst HD (1995) Synthesis 5:577
9. Calixto GMF, Bernegossi J, De Freitas LM, Fontana CR, Chorilli M (2016) Molecules 21:342
10. Cohen DK, Lee PK (2016) Cancers 8:90
11. De Moraes M, Vasconcelos RC, Longo JPF, Muehlmann LA, De Azevedo RB, De Araújo Júnior RF, Araujo AA, De Lisboa Lopes Costa A (2017) J Photochem Photobiol, B 167:208
12. Asadian-Birjand M, Bergueiro J, Wedepohl S, Calderón M (2016) Macromol Biosci 16:1432
13. Bilan R, Nabiev I, Sukhanova A (2016) ChemBioChem 17:2103
14. Fang S, Li C, Lin J, Zhu H, Cui D, Xu Y, Li Z (2016) J Nanomater 2016: Article ID 1082746
15. Narband N, Tubby S, Parkin IP, Gil-Tomás J, Ready D, Nair SP, Wilson M (2008) Curr Nanosci 4:409
16. Netchareonsirisuk P, Puthong S, Dubas S, Palaga T, Komolpis K (2016) J Nanopart Res 18:322
17. Devi R, Kumar M (2012) J Clin Diagn Res 6:577
18. Gengan R, Anand K, Phulukdaree A, Chuturgoon A (2013) Colloids Surf B 105:87
19. Farah MA, Ali MA, Chen SM, Li Y, Al-Hemaid FM, Abou-Tarboush FM, Al-Anazi KM, Lee J (2016) Colloids Surf B 141:158
20. Chung JW, Gerelkhuu Z, Oh JH, Lee YI (2016) Appl Spectrosc Rev 51:678
21. Gurunathan S, Kim JH (2016) Int J Nanomed 11:1927
22. Li ZY, Wu YT, Tseng WL (2015) ACS Appl Mater Inter 7:23708
23. Al-Araji YH, Shneine JK, Ahmed AA (2015) Int J Res Pharm Chem 5:41
24. Kumar S, Sharma R, Kumar S (2014) Chem Sci Trans 3:919
25. Abdelhamid AO, Abbas IM, Abdallah MA, Fahmi AA, Shawali AS (1985) J Heterocycl Chem 22:813
26. Shawali AS, Abdelkhalek AA, Sayed AR (2001) J Chin Chem Soc 48:693
27. Henderson LA (1970) 2,5-Diaryl-1,2,3,4,5,6-hexaazapentalene synthesis. US Patent 3,541,107, Nov 17, 1970; (1971). Chem Abstr 74:65596
28. Abdallah SO, Metwally NH, Anwar HF, Elnagdi MH (2005) J Heterocycl Chem 42:781
29. Tezcan H, Tokay N (2010) Spectrochim Acta A 75:54
30. Tezcan H, Can Ş, Tezcan R (2002) Dyes Pigm 52:121
31. Turkoglu G, Berber H (2016) RSC Adv 6:96065
32. Darby BL, Auguié B, Meyer M, Pantoja AE, Le Ru EC (2015) Nat Photonics 10:40
33. Zhao J, Jensen L, Sung J, Zou S, Schatz GC, Van Duyne RP (2007) J Am Chem Soc 129:7647
34. Lucky SS, Soo KC, Zhang Y (2015) Chem Rev 115:1990
35. Chen CW, Chan YC, Hsiao M, Liu RS (2016) ACS Appl Mater Inter 8:32108
36. Ormond AB, Freeman HS (2013) Materials 6:817
37. Zhou T, Zhan J, Fang W, Zhao Y, Yang Y, Hou X, Zhang Z, He X, Zhang Y, Huang Y, Zhang L (2017) BMC Cancer 17:269
38. Dos Santos CR, Domingues G, Matias I, Matos J, Fonseca I, De Almeida JM, Dias S (2014) Lipids Health Dis 13:16
39. Vitols S, Angelin B, Ericsson S, Gahrton G, Juliusson G, Masquelier M, Paul C, Peterson C, Rudling M, Soderberg-Reid K (1990) Proc Natl Acad Sci USA 87:2598
40. Malik Z, Amit I, Rothmann C (1997) Photochem Photobio 65:389
41. Bharadwaj SD (2002) Asian J Chem 14:767
42. Cory AH, Owen TC, Barltrop JA, Cory JG (1991) Cancer Commun 3:207
43. Scudiero DA, Shoemaker RH, Paull KD, Monks A, Tierney S, Nofziger TH, Currens MJ, Seniff D, Boyd MR (1988) Cancer Res 48:4827
44. Metwally MA, Gouda MA, Harmal AN, Khalil AM (2012) Eur J Med Chem 56:254
45. Kim CK, Ghosh P, Pagliuca C, Zhu Z-J, Menichetti S, Rotello VM (2009) J Am Chem Soc 131:1360
46. Snipstad S, Westrøm S, Mørch Y, Afadzi M, Åslund AK, De Lange Davies C (2014) Cancer Nanotechnol 5:8
47. Schrand AM, Braydich-Stolle LK, Schlager JJ, Dai L, Hussain SM (2008) Nanotechnol 19:235104
48. Asharani PV, Hande MP, Valiyaveettil S (2009) BMC Cell Biol 10:65
49. Mulley G, Jenkins ATA, Waterfield NR (2014) PLoS ONE 9:e94409
50. Gurunathan S, Jeong JK, Han JW, Zhang XF, Park JH, Kim JH (2015) Nanoscale Res Lett 10:35
51. Swanner J, Mims J, Carroll DL, Akman SA, Furdui CM, Torti SV, Singh RN (2015) Int J Nanomed 10:3937
52. Kovacs D, Szoke K, Igaz N, Spengler G, Molnar J, Toth T, Madarasz D, Razga Z, Konya Z, Boros IM, Kiricsi M (2016) Nanomed Nanotechnol 12:601
53. Wang Y, Zu X, Yi G, Luo H, Huang H, Song X (2016) Chin J Chem 34:1321
54. El-Hussein A, Mfouo-Tynga I, Abdel-Harith M, Abrahamse H (2015) J Photochem Photobiol B 153:67
55. Devi HS, Rajmuhon Singh N, Premananda Singh H, David Singh T (2015) J Environ Chem Eng 3:2042
56. Elkhawass EA, Mohallal ME, Soliman MFM (2015) Int J Pharm Pharm Sci 7:94
57. Chen RJ, Chen PC, Prasannan A, Vinayagam J, Huang CC, Chou PY, Weng CC, Tsai HC, Lin SY (2016) Mater Sci Eng C 63:678
58. Cheng Y, Meyers JD, Broome AM, Kenney ME, Basilion JP, Burda C (2011) J Am Chem Soc 133:2583
59. Budesinsky B, Svecova J (1971) Inorg Chem 10:313
60. De Souza ALR, LaRochelle E, Marra K, Gunn J, Davis SC, Samkoe KS, Chapman MS, Maytin EV, Hasan T, Pogue BW (2017) Photodiagn Photodyn 20:227